Numerical inversion of the Laplace–Carson transform applied to homogenization of randomly reinforced linear viscoelastic media

Martin Lévesque, Michael Gilchrist, Nicolas Bouleau, Katell Derrien, Didier Baptiste

Numerical inversion of the Laplace–Carson transform applied to homogenization of randomly reinforced linear viscoelastic media

Martin Lévesque, **Michael D. Gilchrist**,
Nicolas Bouleau, **Katell Derrien**, **Didier Baptiste**

Abstract Homogenization of linear viscoelastic materials is possible using the viscoelastic correspondence principle (VCP) and homogenization solutions obtained for linear elastic materials. The VCP involves a Laplace–Carson Transform (LCT) of the material phases constitutive theories and in most cases, the time domain solution must be obtained through numerical inversion of the LCT. The objective of this paper is to develop and test numerical algorithms to invert LCT which are encountered in the context of homogenization of linear viscoelastic materials. The homogenized properties, as well as the stress concentration and strain localization tensors, are considered. The algorithms suggested have the following two key features: (1) an acceptance criterion which allows to reject solutions of unacceptable accuracy and (2) some algorithms lead to solutions for the homogenized properties where the thermodynamics restrictions imposed on linear viscoelastic materials are encountered. These two features are an improvement over the previous algorithms. The algorithms are tested on many examples and the accuracy of the inversion is excellent in most cases.

Keywords Homogenization · Viscoelasticity · Numerical inversion · Laplace transform

M. Lévesque (✉)
CREPEC, Department of Mechanical Engineering,
École Polytechnique de Montréal, C.P. 6079 succ. Centre-ville,
Montréal, Canada, H3C 3A7
e-mail: martin.levesque@polymtl.ca

M. D. Gilchrist
School of Electrical, Electronic and Mechanical Engineering,
University College Dublin, Belfield, Dublin 4, Ireland

N. Bouleau
Ecole Nationale des Ponts et Chaussées,
6 Avenue Blaise Pascal, Cité Descartes,
Marne-la-Vallée Cedex 2, 77455, France

K. Derrien · D. Baptiste
Laboratoire LIM - ENSAM - Paris,
151 Boulevard de l'Hopital, Paris, 75013, France

1 Introduction

Homogenization allows the global mechanical properties of heterogeneous materials to be predicted based on knowledge of the microstructure. Numerical approaches such as finite element simulations of the microstructure or analytical models exist to accomplish this task. Analytical models have the advantage of rapid execution (when compared to numerical methods) but have mostly been applied to materials with random microstructures. Such models are based on Eshelby's ellipsoidal inclusion problem [1] and use various hypotheses to calculate the homogenized properties of the whole material. The earliest results were obtained for linear elastic materials (see for example [2]). Thanks to the Viscoelastic correspondence principle (VCP), such results can be extended to linear viscoelastic problems (see [3–8] for examples) and to non linear viscoelastic problems (see [9–13] a for examples). The VCP involves a Laplace–Carson transformation of the linear viscoelastic constitutive theories of the constituent phases. Then, the homogenized properties of the heterogeneous viscoelastic material are obtained in the Laplace–Carson space. The time domain solution is then obtained by the inverse Laplace–Carson transformation.

Except for very particular cases, this inverse transformation has to be carried out numerically. The objective of this paper is to develop algorithms to perform this task which improve on existing algorithms.

To the knowledge of the authors, most of the previous algorithms did not suggest an acceptance criterion for the result of the inversion. It is therefore possible with these algorithms to obtain a solution with unacceptable accuracy. When the effective properties are considered, it might be required that the result of the inversion meets the thermodynamics requirements imposed on linear viscoelastic materials. This might be the case, for example, if the homogenized properties are to be used in a commercial Finite Element package or in other continuum mechanics problems. To the knowledge of the authors, none of the previous algorithms addressed this issue. So, the contribution of this paper is the development of numerical Laplace–Carson algorithms for which the solution meets the requirements of thermodynamics (for the homogenized properties) as well as acceptance criteria to ensure the quality of the inversion. Algorithms are suggested for the effective properties as well as for the stress concentration and strain localization functions. Algorithms that do and that do not enforce the thermodynamics requirements are also presented. Finally, the performance of the algorithms are studied on many simulations. Since the algorithms introduced in this paper have different features, their results were not compared with those obtained with the previous algorithms. Our objective was to only validate the quality of the inversions obtained with the algorithms introduced in this paper.

The paper is divided as follows. First, background information related to the homogenization of viscoelastic materials and the existing inverse Laplace–Carson transformation algorithms are presented. This section serves to define the required features of the algorithms proposed in this paper. Next, the algorithms are developed. Finally, the algorithms are validated for selected cases and their performance is discussed.

2 Background

2.1 Linear viscoelastic constitutive theories

The thermodynamics of irreversible processes has been used by many authors to derive constitutive laws for linear viscoelastic materials. The theory developed by Biot [14] leads to a linear system of differential equations the solution of which leads to the constitutive law. The behaviour of a linear viscoelastic material is given, in the most general form, by a convolution integral of the type:

$$\boldsymbol{\sigma}(t) = \int_0^t \mathbf{C}(t-\tau) : \mathrm{d}\boldsymbol{\varepsilon}(\tau) \tag{1a}$$

$$\boldsymbol{\varepsilon}(t) = \int_0^t \mathbf{S}(t-\tau) : \mathrm{d}\boldsymbol{\sigma}(\tau) \tag{1b}$$

where $\mathbf{C}(t)$ is the relaxation modulus and $\mathbf{S}(t)$ is the creep compliance. When the set of state variables considered by Biot [14] is considered as a continuum set, then the most general shape of $\mathbf{C}(t)$ and $\mathbf{S}(t)$ are given by [15,16]:

$$C_{ij}(t) = \int_{0^+}^{\infty} \exp\left[-\tau t\right] \mathrm{d}\check{C}_{ij}(\tau) + C'_{ij}\delta(t) + C''_{ij} \tag{2a}$$

$$S_{ij}(t) = \int_{0^+}^{\infty} \left(1 - \exp\left[-\tau t\right]\right) \mathrm{d}\check{S}_{ij}(\tau) + S'_{ij}t + S''_{ij} \tag{2b}$$

where $\mathbf{C}'$,$\mathbf{C}''$,$\mathbf{S}'$, and $\mathbf{S}''$ are constant positive semi-definite matrices, $\mathrm{d}\check{\mathbf{C}}(\tau)$ and $\mathrm{d}\check{\mathbf{S}}(\tau)$ are positive semi-definite matrices of σ-finite measures on $\mathbb{R}_+^*$, and $\delta(t)$ is the Dirac delta function. In addition, thermodynamics imposes that $\mathrm{d}\check{\mathbf{C}}(\tau)$ and $\mathrm{d}\check{\mathbf{S}}(\tau)$ be such that [15,16]:

$$\int_0^{\infty} \frac{1}{1+\tau} |\mathrm{d}\check{C}_{ij}|(\tau) \leq +\infty \tag{3a}$$

$$\int_0^{\infty} \frac{\tau}{1+\tau} |\mathrm{d}\check{S}_{ij}|(\tau) \leq +\infty \tag{3b}$$

Many constitutive theories fulfilling these conditions can be generated. For simplicity, let's consider the creep compliance $s(t)$ of a 1D material where $s' = s'' = 0$. If $\mathrm{d}\check{s}(\tau)$ is considered as a finite series of Dirac impulses, then:

$$\mathrm{d}\check{s}_1(\tau) = \sum_{n=1}^{N} a_n \delta(\tau - \tau_n) \quad \text{leads to}$$

$$s_1(t) = \sum_{n=1}^{N} a_n \left(1 - \exp[-t\tau_n]\right) \tag{4}$$

which is the classical Prony series. Continuous measures can also be used, for example:

$$\mathrm{d}\check{s}_2(\tau) = \frac{a}{b^2} \exp\left[-\frac{\tau}{b}\right] \mathrm{d}\tau \rightsquigarrow s_2(t) = \frac{at}{1+bt} \tag{5}$$

$$\mathrm{d}\check{s}_3(\tau) = \frac{c}{\tau} \exp\left[-\frac{\tau}{d}\right] \mathrm{d}\tau \rightsquigarrow s_3(t) = c \log\left(1+dt\right) \tag{6}$$

where a, b, c, $d > 0$. It is interesting here to note that $s_2(t)$ is bounded while $s_3(t)$ is not. The functions, like the

s_i, obtained here are called *Bernstein functions* and have the following property [16]: If φ and ψ are Bernstein and $\psi(0) = 0$ then the function composition $\varphi \circ \psi : t \to \varphi(\psi(t))$ is Bernstein. For example:

$$s_4 = s_3(s_2(t)) = c \log\left(1 + d\frac{at}{1+bt}\right) \tag{7}$$

This last property shows how new behaviour laws can be created. There are a wide range of possible combinations; far more than those modelled with a finite, or even infinite, number Dirac impulses.

2.2 Homogenization

In the case of linear elastic materials where the properties are constant in a given phase, the homogenized stiffness $\bar{\mathbf{C}}$ and compliance $\bar{\mathbf{S}}$ are given by:

$$\bar{\mathbf{C}} = \sum_{r=0}^{R-1} c_r \mathbf{C}_r : \mathbf{B}_r \tag{8a}$$

$$\bar{\mathbf{S}} = \sum_{r=0}^{R-1} c_r \mathbf{S}_r : \mathbf{A}_r \tag{8b}$$

where the subscript r refers to a given phase, c is a volume fraction, R is the total number of phases, $\mathbf{C}$ and $\mathbf{S}$ are stiffnesses and compliances and $\mathbf{A}$ and $\mathbf{B}$ are the so called strain localization and stress concentration tensors. These two tensors are, in fact, functions of the mechanical properties, shape and orientation of each phase. Different theories, called *homogenization schemes* (e.g. Self-Consistent [17], Mori-Tanaka [18], etc.), lead to different expressions of $\mathbf{A}$ and $\mathbf{B}$. These tensors are also used for computing the spatial average stress $\bar{\boldsymbol{\sigma}}_r$ and deformation $\bar{\boldsymbol{\varepsilon}}_r$ in a given phase from:

$$\bar{\boldsymbol{\sigma}}_r = \mathbf{B}_r : \boldsymbol{\sigma} \tag{9a}$$

$$\bar{\boldsymbol{\varepsilon}}_r = \mathbf{A}_r : \mathbf{E} \tag{9b}$$

where $\boldsymbol{\sigma}$ and $\mathbf{E}$ are the applied macroscopic stress and strain tensors on the heterogeneous material.

2.3 Material symmetry

When a material exhibits material symmetry, relationships exist between the components of $\mathbf{C}$ or $\mathbf{S}$. In the general case, a material has 21 independent components. This number is reduced to 5 in the case of transverse isotropy, to three in the case of cubic symmetry and to two in the case of isotropy. For these material symmetries, it is possible to derive expressions greatly simplifying the calculations involved in the homogenization problem. When developing the algorithms of the present work, advantage is taken of such simplifications and it is convenient, therefore, to list them here.

2.3.1 Isotropy or cubic symmetry

In the case of isotropy, any tensor can be described using Hill's short hand notation so that we have [19,20]:

$$\mathbf{G} = \alpha\mathbf{J} + \beta\mathbf{K} \quad \text{with} \quad \mathbf{J} = \frac{1}{3}\boldsymbol{i}\otimes\boldsymbol{i} \text{ and } \mathbf{K} = \mathbf{I} - \mathbf{J} \tag{10}$$

where $\boldsymbol{i}$ and $\mathbf{I}$ are the second and fourth order identity tensors. In the case of cubic symmetry, we have:

$$\mathbf{G} = \alpha\mathbf{J} + \beta\mathbf{K_a} + \gamma\mathbf{K_b} \quad \text{with} \quad \Lambda_{iiii} = 1, \quad \mathbf{K_a} = \boldsymbol{\Lambda} - \mathbf{J} \quad \text{and} \quad \mathbf{K_b} = \mathbf{I} - \boldsymbol{\Lambda} \tag{11}$$

Simple calculation rules follow from these definitions which means that the result of homogenization is given in terms of $\{\alpha, \beta, \gamma\}$. For thermodynamics stability, $\mathbf{G}$ must be positive semi-definite (i.e. all its eigenvalues are positive). We denote such a condition by $\mathbf{G} \geq 0$. For these material symmetries, having $\mathbf{G} \geq 0$ implies that $\alpha, \beta, \gamma \geq 0$.

2.3.2 Transverse isotropy

As with isotropy or cubic symmetry, a transversely isotropic tensor can be written using a short hand notation. Let's introduce [19,20]:

$$\boldsymbol{i_T} = \boldsymbol{i} - \boldsymbol{h}\otimes\boldsymbol{h}, \quad \mathbf{E_L} = \boldsymbol{h}\otimes\boldsymbol{h}\otimes\boldsymbol{h}\otimes\boldsymbol{h}, \quad \mathbf{J_T} = \frac{1}{2}\boldsymbol{i_T}\otimes\boldsymbol{i_T},$$

$$\mathbf{K_E} = \frac{1}{6}(2\boldsymbol{h}\otimes\boldsymbol{h} - \boldsymbol{i_T})\otimes(2\boldsymbol{h}\otimes\boldsymbol{h} - \boldsymbol{i_T}), \quad \mathbf{K_T} = \mathbf{I_T} - \mathbf{J_T},$$

$$\mathbf{K_L} = \mathbf{K} - \mathbf{K_T} - \mathbf{K_E}, \text{ and } \mathbf{F} = \frac{1}{\sqrt{2}}\boldsymbol{i_T}\otimes\boldsymbol{h}\otimes\boldsymbol{h} \tag{12}$$

where $\boldsymbol{h}$ is a vector along the axis of transverse isotropy and $\mathbf{I_T}$ is the fourth order identity tensor in the transverse plane.[1] Then, a fourth order, symmetric, transversely isotropic tensor is given by:

$$\mathbf{G} = \alpha\mathbf{E_L} + \beta\mathbf{J_T} + \gamma(\mathbf{F} + \mathbf{F}^{\mathsf{T}}) + \delta\mathbf{K_T} + \delta'\mathbf{K_L} \tag{13}$$

In order to have $\mathbf{G} \geq 0$, it is necessary that $\alpha, \beta, \delta, \delta' \geq 0$ and $\gamma^2 \leq \alpha\beta$.

2.3.3 General anisotropy

A definite semi-positive matrix is a matrix for which all its eigenvalues are positives. We recall that any symmetric positive semi-definite matrix in a particular base can

[1] This extracts the components of a second order tensor which are in the plane perpendicular to the axis of transverse isotropy.

be given by:

$$\mathbf{G} = \mathbf{R}^{\mathrm{T}}\mathbf{D}\mathbf{R} \tag{14}$$

where $\mathbf{D}$ is a diagonal matrix containing the eigenvalues of $\mathbf{G}$ and $\mathbf{R}$ is an orthogonal matrix containing the eigenvectors of $\mathbf{G}$. $\mathbf{R}$ is a rotation matrix, which in our case, has 6 dimensions. It can be shown in n dimensions that a general rotation matrix can be given as a sequence of simple rotations in a plane. For example,

$$\mathbf{R}(\theta_1) = \begin{pmatrix} \cos\theta_1 & \sin\theta_1 & 0\,0\,0\,0 \\ -\sin\theta_1 & \cos\theta_1 & 0\,0\,0\,0 \\ 0 & 0 & 1\,0\,0\,0 \\ 0 & 0 & 0\,1\,0\,0 \\ 0 & 0 & 0\,0\,1\,0 \\ 0 & 0 & 0\,0\,0\,1 \end{pmatrix} \tag{15}$$

is a rotation in the 1–2 plane. In 6 dimensions, there can be 15 different plane rotations and the general rotation matrix is given by:

$$\mathbf{R} = \prod_{n=1}^{15} \mathbf{R}(\theta_n) \tag{16}$$

In total, we have 15 rotation angles and 6 eigenvalues for a total of 21 independent components. Randomly generating fourth order symmetric anisotropic tensors to meet the condition $\mathbf{G} \geq 0$ can be achieved by generating the 15 angles randomly, the 6 positive eigenvalues, assembling the rotation matrices and computing the tensor according to Eq. (14).

2.4 Viscoelastic correspondence principle

The Laplace–Carson transform (LCT) of a function is defined by:

$$g^*(p) \equiv p \int_{-\infty}^{t} g(t)\exp[-pt]\mathrm{d}t \tag{17}$$

When definition (17) is applied to the behaviour laws in Eq. (1) then:

$$\boldsymbol{\sigma}^*(p) = \mathbf{C}^*(p) : \boldsymbol{\varepsilon}^*(p) \tag{18a}$$

$$\boldsymbol{\varepsilon}^*(p) = \mathbf{S}^*(p) : \boldsymbol{\sigma}^*(p) \tag{18b}$$

which is analogous to a linear elastic behaviour law. Consider two problems where the geometry, area of application and type of boundary conditions are identical, but in one case the material is linear elastic and in the other case, the material is linear viscoelastic. If the LCT is applied to the viscoelastic problem, it becomes similar to the elastic problem in the Laplace–Carson space. Therefore, if the solution is known for the elastic problem, the solution of the viscoelastic problem can be obtained in the Laplace–Carson space by replacing the elastic properties with the LCT of the viscoelastic properties and by replacing the loadings by their corresponding LCT [3–8]. In order to obtain the time domain solution, the inverse LCT must be applied. The correspondence principle can also be invoked to calculate the relaxation modulus when the creep compliance is known (and vice versa).

Many authors have used this correspondence principle to solve the homogenization problem for linear viscoelastic materials (for example [3–8]. Equations (8) become:

$$\bar{\mathbf{C}}^* = \sum_{r=0}^{R-1} c_r \mathbf{C}_r^* : \mathbf{B}_r^* \tag{19a}$$

$$\bar{\mathbf{S}}^* = \sum_{r=0}^{R-1} c_r \mathbf{S}_r^* : \mathbf{A}_r^* \tag{19b}$$

For some very particular cases, analytical expressions for $\bar{\mathbf{C}}(t)$ or $\bar{\mathbf{S}}(t)$ can be obtained. However, most of the time, situations arise when the analytical LCT inversion of $\bar{\mathbf{C}}^*(p)$ or $\bar{\mathbf{S}}^*(p)$ is difficult. When the microstructure becomes more complicated (anisotropic phases, different orientations of reinforcements, etc.), Eshelby's solution must be evaluated numerically (see, for example, Gavazzi and Lagoudas [21]). In such cases, $\bar{\mathbf{C}}^*(p)$ and $\bar{\mathbf{S}}^*(p)$ are only known numerically and consequently their time domain expressions can only be obtained numerically. Stresses and strains within a given phase are required when homogenizing non linear viscoelastic materials to perform a relevant linearization [9–13]. Therefore, the time expressions of $\mathbf{A}_r$ and $\mathbf{B}_r$ may also be required.

2.5 Existing algorithms

Consider a one-dimensional function $g(t)$. The analytical expression of the inverse LCT is given by:

$$g(t) = \frac{1}{2\pi i}\int_{c-i\infty}^{c+i\infty} \frac{1}{p} g^*(p)\exp[pt]\mathrm{d}p \tag{20}$$

which is an integral in the complex plane. For simple analytical expressions for $g^*(p)$ the integration can be carried out analytically (see [6,8] for example).

As pointed out by Davies and Martin [22] there seems to be two approaches to calculating the inverse LCT, namely (i)those where the integration in Eq. (20) is carried out numerically and (ii)those where $g(t)$ is approximated by an appropriate series of functions. This second approach can be quite useful, especially when some information is known regarding the shape of $g(t)$. In addition, this approach can be computationally

efficient if the approximate function is used many times in subsequent calculations because the computational effort is spent only once on its evaluation. In common with many other authors (see [4,5,11] for example), we have used such an approach.

Assume for simplicity that $\tilde{g}(t)$ represents the transient part of one ij component of $\bar{\mathbf{C}}(t)$ or $\bar{\mathbf{S}}(t)$. Under the assumption that the homogenization scheme leads to a thermodynamically acceptable material,

$$\tilde{g}(t) = \int_{0^+}^{\infty} \zeta \exp[-\tau t] \mathrm{d}\check{g}(\tau) \tag{21}$$

where $\zeta = 1$ for a relaxation modulus and $\zeta = -1$ for a creep compliance (see Eq. (2)). Let $\hat{g}(t)$ be an approximate of the function $\tilde{g}(t)$. When defining:

$$\hat{g}(t) = \sum_{n=1}^{N} g_n \exp[-t\tau_n] \tag{22}$$

and

$$\mathrm{Err}^2 = \int_0^{\infty} \left[\tilde{g}(t) - \hat{g}(t)\right]^2 \mathrm{d}t \tag{23}$$

Shapery [23] has shown that Err^2 is minimized when:

$$\tilde{g}^*(p = \tau_n) = \hat{g}^*(p = \tau_n) \quad \text{for } n = \{1, 2, \ldots, N\} \tag{24}$$

With this result, he introduced his *collocation method* where the τ_n are determined a priori and the g_n are determined so that the N equations at Eq. (24) are satisfied. So far, to the knowledge of the authors, this method has been the most popular for homogenization problems.

Shapery has also shown that (with $\hat{g}(t)$ defined as per Eq. (22)):

$$\begin{aligned} &\text{if } \tilde{g}^{\mathcal{L}}(\mathrm{Re}(p)) = \hat{g}^{\mathcal{L}}(\mathrm{Re}(p)) \quad \forall\ \mathrm{Re}(p) > 0 \text{ then} \\ &\qquad \tilde{g}(t) = \hat{g}(t) \quad \forall\ t \geq 0 \end{aligned} \tag{25}$$

where $\tilde{g}^{\mathcal{L}}$ is the Laplace transform of $\tilde{g}(t)$ and $\mathrm{Re}(p)$ extracts the real part of p. Due to its definition, this result is also valid for the LCT. Following similar arguments, Cost and Becker [24] introduced their *multidata method*. They assumed the same form for $\hat{g}(t)$ and also fixed the τ_n *a priori*. Rather than collocating $\hat{g}^*(p)$ at specific values of p , the authors performed a least squares fit of $\hat{g}^*(p)$ on known values of $\tilde{g}^*(p)$. The g_n thus obtained are those minimizing the sum of the squared differences between $\hat{g}^*(p)$ and $\tilde{g}^*(p)$ at a total number S of points p_s.

It is worthwhile mentioning the *direct inversion method* also introduced by Schapery [23]. By a relevant change of variables and assuming that $g(t)$ is smooth and varies slowly with time, the time response of g can be directly approximated with:

$$g(t) \simeq g^*\left(p = \frac{10^{w_0}}{t}\right) \tag{26}$$

where w_0 is a parameter chosen according to the type of function $g(t)$. This method is computationally efficient since it establishes a direct correspondence between the values of t and p. Brenner et al. [12] used such a procedure for the creep response of polycrystals and obtained very good results.

There are drawbacks associated with each of these algorithms:

1. For the collocation and direct methods, it is not possible to estimate *a priori* the accuracy of the inversion. For the multidata method it is possible to calculate a coefficient of determination, R^2, which gives an indication of the quality of the inversion in the Laplace–Carson space.
2. For the collocation and multidata methods, the τ_n are chosen *a priori*. The quality of the inversion will be affected by this choice. Authors who have used the collocation method ([4,5,11] for example) suggested different numbers of τ_n and different distributions (the τ_n are equally distributed or equally distributed on a log scale, etc.). These suggestions were derived by a trial and error and not from a systematic study.
3. For the multidata and the collocation methods, there is no constraint on the values of the g_n parameters (see Eq. (22)) of $\hat{g}(t)$. The g_n can therefore take negative or positive values which can lead to oscillatory $\hat{g}(t)$. From a thermodynamic point of view, this would not be acceptable if $g(t)$ represents a shear creep compliance for an isotropic material, for example.

The algorithms that are introduced in this paper address these issues. Some enforce the thermodynamics restrictions while others do not. Algorithms where the thermodynamics restrictions are not enforced are generally less computationally demanding. The algorithms are applied to the homogenized properties as well as to the stress concentration and deformation localization tensors.

3 Suggested algorithms

The algorithms proposed in this paper are presented in this section. Those for the homogenized properties

and for tensors $\mathbf{A}$ and $\mathbf{B}$ are presented in two different sections. For the homogenized properties, algorithms that do and that do not enforce the thermodynamics requirements are presented. All these algorithms share common characteristics which are presented first.

It should be noted that this section presents the algorithms for generating an inversion. The algorithms used to accept or reject a solution are presented in Sect. 4.

3.1 Common characteristics

All the algorithms share the following characteristics:

1. The permanent part of the time response is first evaluated by limit values theorems. The transient part is then extracted and the algorithms aim to approximate this transient part. If $g(t)$ is the function to be inverted then $\tilde{g}(t)$ is its transient part.
2. They involve a least squares curve fit in the Laplace–Carson space for each independent transient components of $\bar{\mathbf{C}}^*$, $\bar{\mathbf{S}}^*$, $\mathbf{A}^*$ and $\mathbf{B}^*$. g denotes a given independent component of these tensors. The least squares curve fit aims to find the function $\hat{g}(t)$ minimizing the (discrete) square of the error between $\tilde{g}^*(p)$ and $\hat{g}^*(p)$. The following problem has to be solved:

$$\inf_{\hat{g}^*} E^2 = \inf_{\hat{g}^*} \sum_{s=1}^{S} \left[\tilde{g}^*(p_s) - \hat{g}^*(p_s)\right]^2 \tag{27}$$

3. The points p_s used to compute E^2 are carefully chosen.
4. The approximate function is of the type:

$$\hat{g}(t) = \sum_{n=1}^{N} g_n \exp[-t\tau_n] \tag{28}$$

5. The τ_n are chosen a priori. The g_n are the unknowns and they minimize E^2. They are determined by each algorithm. Attempts were made to also optimize the τ_n but this led to numerical difficulties and was subsequently abandoned.

The algorithms can be regarded as an improved multidata method where the points used in the curve fit and the τ_n are carefully chosen.

3.1.1 Determination of the LCT of the transient part of $\bar{\mathbf{C}}(t)$ and $\bar{\mathbf{S}}(t)$

The algorithms introduced in this paper aim to approximate the transient part of the function that is to be inverted. Assuming that the homogenized properties meet the thermodynamics requirements, the permanent parts of Eq. (2) are the viscous flow and the elastic response. When considering a relaxation modulus and using the limit value theorem, the following result can be obtained:

$$\lim_{t\to\infty} \bar{\mathbf{C}}(t) = \lim_{p\to 0} \bar{\mathbf{C}}^*(p) = \bar{\mathbf{C}}'' \tag{29}$$

It should be noted that we assumed $\bar{\mathbf{C}}' = \mathbf{0}$. The case where $\bar{\mathbf{C}}' \neq \mathbf{0}$ leads to an infinite stress when a strain is suddenly applied. Real materials do not exhibit such behavior and this hypothesis, although it limits the domain of application of our algorithm, is reasonable.

When considering a creep compliance, the following results can be obtained:

$$\lim_{t\to 0} \bar{\mathbf{S}}(t) = \bar{\mathbf{S}}'' = \lim_{p\to\infty} \bar{\mathbf{S}}^*(p) \tag{30a}$$

$$\lim_{t\to\infty} \frac{\mathrm{d}}{\mathrm{d}t}\bar{\mathbf{S}}(t) = \bar{\mathbf{S}}' = \lim_{p\to 0} p\bar{\mathbf{S}}(p) - p\bar{\mathbf{S}}'' \tag{30b}$$

$$\lim_{t\to\infty} \bar{\mathbf{S}}(t) - t\bar{\mathbf{S}}' - \bar{\mathbf{S}}'' = \lim_{p\to 0} \bar{\mathbf{S}}^*(p) - \frac{\bar{\mathbf{S}}'}{p} - \bar{\mathbf{S}}'' = \int_{0^+}^{\infty} \mathrm{d}\check{\bar{\mathbf{S}}}(\tau) \tag{30c}$$

The transient parts can be obtained from Equations (29) and (30) as:

$$\left[\int_{0^+}^{\infty} \exp\left[-t\tau\right] \mathrm{d}\check{\bar{\mathbf{C}}}(\tau)\right]^* = \bar{\mathbf{C}}^*(p) - \bar{\mathbf{C}}'' = \tilde{\bar{\mathbf{C}}}^*(p) \tag{31a}$$

$$\left[\int_{0^+}^{\infty} \exp\left[-t\tau\right] \mathrm{d}\check{\bar{\mathbf{S}}}(\tau)\right]^* = \bar{\mathbf{S}}'' + \int_{0^+}^{\infty} \check{\bar{\mathbf{S}}}(\mathrm{d}\tau) + \frac{\bar{\mathbf{S}}'}{p} - \bar{\mathbf{S}}^*(p) = \tilde{\bar{\mathbf{S}}}^*(p) \tag{31b}$$

In the sequel, $\tilde{g}^*(p)$ refers to an ij component of $\tilde{\bar{\mathbf{C}}}^*(p)$ or $\tilde{\bar{\mathbf{S}}}^*(p)$.

3.1.2 Determination of the points p_s used for the algorithms

The objective of this part of the algorithm is to choose the points p_s used in the least squares fit. These points should be such that $\tilde{g}^*(p_s)$ represents adequately the variation of $\tilde{g}^*(p)$ for $p \in [0, \infty[$.

In the case of the homogenized properties, due to the definition of the transient part (see Eq. (21)), we make

the assumption that:

$$\lim_{t\to\infty} \tilde{g}(t) = 0 \tag{32}$$

Due to the limit value theorem, we have that $\lim_{p\to 0} \tilde{g}^*(p) = 0$. If $\tilde{g}(t)$ represents an *ii* (i.e. diagonal) component of $\tilde{\tilde{\mathbf{C}}}(t)$ or $\tilde{\tilde{\mathbf{S}}}(t)$ then $\tilde{g}(t)$ will decrease monotonically from $\tilde{g}(0) \geq 0$ to 0 for t going from 0 to ∞ (this property comes from the thermodynamics restrictions). Due to the definition of the LCT, $\tilde{g}^*(p)$ will increase monotonically from 0 to $\lim_{p\to\infty} \tilde{g}^*(p) = \Omega$ for p going from 0 to ∞. Figure 1 shows a typical plot for such a function. The points p_s are such that the entire variation domain of the function (i.e. the y axis) to be inverted has an influence on the computation of E^2. Figure 1 shows the distribution of these points.

For the other components of $\bar{\mathbf{C}}(t)$ and $\bar{\mathbf{S}}(t)$ or for the tensors $\mathbf{A}(t)$ and $\mathbf{B}(t)$, $\tilde{g}(t)$ is not necessarily positive or monotonic. Figure 2 shows a possible plot for $\tilde{g}^*(p)$ for such components. From the figure, it can be seen that the function is negative and shows a point where the sign of the slope of the curve changes (i.e. the bump on the curve). In order to obtain an adequate discrete representation of $\tilde{g}^*(p)$ it is necessary to take into account these curvature changes. Figure 2 shows a set of points p_s which leads to a discrete representation of $\tilde{g}^*(p)$ where the curve segment between each bump is discretized with ρ points. The algorithm used to calculate these points is given below as Algorithm 1. Equations (33–35) are non linear problems requiring numerical methods. When $\tilde{g}^*$ is known analytically, these equations can be solved by standard bracketing algorithms [25] since there is only one unknown for each problem. When $\tilde{g}^*(p)$ is only known numerically, Equations

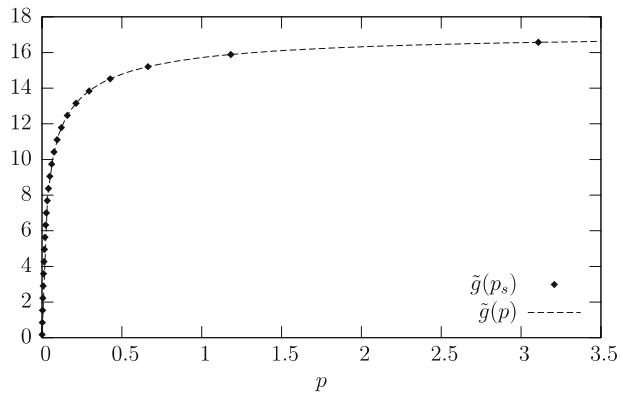

Fig. 1 Typical LCT of a diagonal term of $\tilde{\tilde{\mathbf{C}}}(t)$ or $\tilde{\tilde{\mathbf{S}}}(t)$. The *symbols* represent the points used in the least squares fit

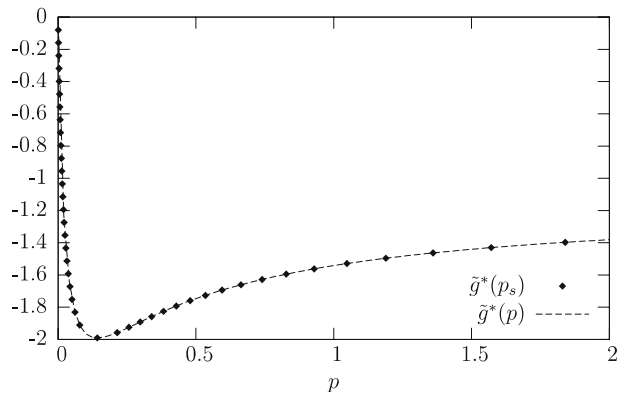

Fig. 2 A possible LCT of a off-diagonal term of $\tilde{\tilde{\mathbf{C}}}(t)$ or $\tilde{\tilde{\mathbf{S}}}(t)$ or any transient component of $\mathbf{A}(t)$ or $\mathbf{B}(t)$. The *symbols* represent the points used in the least squares fit

Algorithm 1 Computation of the p_s used in Equation (27)

1: Calculate the points b_y, with $y = \{1, 2, \ldots, B\}$ solving:

$$\frac{\mathrm{d}\tilde{g}^*}{\mathrm{d}p}(b_y) = 0 \quad \text{for } b_y \in [0, \infty[\tag{33}$$

The number of points meeting this condition is B.
2: **if** $B = 0$ **then** {when there is no oscillation}
3: $S = 2\rho$
4: **for** $s = 1$ to $s = S$ **do**
5: p_s solves the following equation:

$$\tilde{g}^*(p_s) = \frac{s}{S}\left(\Omega + \kappa\xi\,|\Omega|\right) \quad \text{for} \quad p_s > 0 \tag{34}$$

where $0 < \xi < 1$ and where $\kappa = 1$ if $\lim_{p\to\infty} \tilde{g}^*(p) = \Omega$ is approached from above and $\kappa = -1$ if Ω is approached from below.
6: **end for**
7: **else** {when there is at least one oscillation}
8: {Computing the points representing the ordinate variation }
9: $b_0 = 0$ and b_{B+1} solves $\tilde{g}^*(b_{B+1}) = \tilde{g}^*(b_B) + (1-\xi)\left(\Omega - \tilde{g}^*(b_B)\right)$.
10: **for** $y = 1$ to $y = B + 1$ **do**
11: $p_{\rho\times y} = b_y$
12: **for** $z = 1$ to $z = \rho - 1$ **do**
13: p_s solves the following equation:

$$\tilde{g}^*(p_{\rho\times(y-1)+z}) = \tilde{g}^*(b_{y-1}) + \frac{z}{\rho}\left[\tilde{g}^*(b_y) - \tilde{g}^*(b_{y-1})\right]$$

$$\text{for } p_{\rho\times(y-1)+z} \in [b_{y-1}, b_y] \tag{35}$$

14: **end for**
15: **end for**
16: {Computing the points representing the abscissa variation}
17: $\eta = \text{int}\left[\log p_S\right] - \text{int}\left[\log p_1\right] + 2$ (int returns the integer part of its argument).
18: **for** $y = 1$ to $y = \eta \times \vartheta$ **do**
19: $p_{\rho\times(B+1)+y} = 10^{\log p_1 + \frac{y}{\eta\times\vartheta+1}(\log p_{\rho\times(B+1)} - \log p_1)}$
20: **end for**
21: $S = (B+1)\times\rho + \eta\times\vartheta$ is the total number of points.
22: **end if**
23: ρ represents the number of points between two bumps. If N is the number of terms in $\hat{g}(t)$ then we used:

$$\rho = \begin{cases} 25 & \text{if } N \leq 15 \\ 2N & \text{if } N > 15 \end{cases} \tag{36}$$

24: We have used $\xi = 0.02$.
25: We have used $\vartheta = 10$ (i.e. the number of points per decade along the abscissa).

(34, 35) pose no particular problem. On the other hand, the homogenization does not lead to expressions for the derivatives of $\tilde{g}^*(p)$ with respect to p. In this case, the derivative at Equation (33) can be approximated by a centered difference and the problem can be solved with a bracketing algorithm [26] (see p. 110). In addition to these points capturing the ordinate variation of $\tilde{g}^*(p)$, we added points capturing the abscissa variation of $\tilde{g}^*(p)$. As can be seen from Figure 1 there can be a large distance between two consecutive p_s along the abscissa axis when $\tilde{g}^*(p)$ approaches its asymptotic value. In some cases the approximate function oscillated between these points and one possible explanation was that there were not enough points in the least squares computation to attract $\hat{g}^*(p)$ toward $\tilde{g}^*(p)$. It was found that adding a certain number of points per decade between p_1 and $p_{\rho\times(B+1)}$ (see Algorithm 1) improved the performance of the inversions.

3.2 Algorithms for the homogenized properties when the thermodynamics restrictions are not enforced

When thermodynamics restrictions are not enforced, each independent component of $\bar{\mathbf{C}}$ or $\bar{\mathbf{S}}$ can be treated individually. For an isotropic material, only two quantities have to be treated whilst for a general anisotropic material 21 components have to be treated.

The first step of the algorithm is to identify the permanent regime quantities of the function to be inverted, as detailed in Sect. 3.1.1. Then, it is possible to define the transient part $\tilde{g}^*(p)$ for each independent component. Once this is done, the points p_s can be computed for each independent component as explained in Sect. 3.1.2.

The next step is to define the fitting function $\hat{g}(t)$ (see Eq. (28)). As mentioned before, the τ_n are determined *a priori*. If N represents the number of terms in $\hat{g}(t)$, the τ_n we used were defined as follows:

$$\tau_n = 10^{\log[(1+\theta)\tau_{\min}]+n\frac{\log[(1-\theta)\tau_{\max}]-\log[(1+\theta)\tau_{\min}]}{N-1}} \quad \text{for } n = \{0,1,\ldots,N-1\} \tag{37}$$

Equation (37) distributes uniformly, on a logarithmic scale, the τ_n between $(1+\theta)\tau_{\min}$ and $(1-\theta)\tau_{\max}$. This choice of logarithmic distribution is motivated by the fact that real materials are usually defined by series of exponentials with one term per decade. The parameter θ controls the range over which the τ_n are distributed between two bounding values $\tau_{\min}$ and $\tau_{\max}$. The choice of these bounds is motivated by the principles of the collocation method. With the collocation method, one sure way to obtain an approximate function which represents adequately the function to be inverted in the LC space is to choose collocation times (i.e. the τ_n) so that they discretize adequately the function to be inverted over all its variation range. This comes from the fact that the collocation method can be interpreted as an interpolation of the approximate function on the function that is being inverted. If increasingly more collocation times are used then $\hat{g}^*(p)$ will pass by more and more points of $\tilde{g}^*(p)$. The points p_s were calculated so that they provide a relevant discretization of $\tilde{g}^*(p)$ over all its range of variation. Therefore, p_1 and $\max\{p_s\}$, would seem an appropriate choice for $\tau_{\min}$ and $\tau_{\max}$.

With this choice, we can define the least squares problem to be solved as:

$$\inf_{g_n} E^2 = \inf_{g_n} \sum_{s=1}^{S} \left[\tilde{g}^*(p_s) - \hat{g}^*(p_s)\right]^2 \quad \text{with}$$

$$\sum_{n=1}^{N} g_n = \lim_{p\to\infty} \tilde{g}^*(p) \tag{38}$$

The constraint forces $\lim_{p\to\infty} \hat{g}^*(p) = \lim_{p\to\infty} \tilde{g}^*(p)$. Due to the limit value theorem, this forces $\lim_{t\to 0} \hat{g}(t) = \lim_{t\to 0} \tilde{g}(t)$. It was found by trial and error that this constraint improved the quality of the inversion. It should be noted that Masson [27] used such a constraint in his modified collocation algorithm. This optimization problem can be solved by a Lagrange Multiplier technique [26] or with a penalty function (this is the method used in this paper). Owing to the nature of $\hat{g}(t)$, this optimization problem is linear and can be solved at little computational cost.

This algorithm has only two parameters that can be varied: N the number of terms in $\hat{g}(t)$ and θ which controls the range over which the τ_n are distributed.

3.3 Algorithms for the homogenized properties when the thermodynamics restrictions are enforced

When thermodynamics restrictions are enforced, the problem becomes more complex because the independent components of $\tilde{\bar{\mathbf{C}}}(t)$ or $\tilde{\bar{\mathbf{S}}}(t)$ cannot be treated separately. The approximate function $\hat{g}(t)$ becomes a tensor function $\hat{\mathbf{G}}(t)$:

$$\hat{\mathbf{G}}(t) = \sum_{n=1}^{N} \mathbf{G}_n \exp[-\tau_n t] \tag{39}$$

where, according to the thermodynamics restrictions, $\mathbf{G}_n$ is positive semi-definite. Therefore, a relationship that must be satisfied exists between each component of $\mathbf{G}_n$. When the material exhibits material symmetry, very simple relationships can be derived, which simplify greatly

the whole problem. The series of algorithms that we develop here are for specific degrees of material symmetry and take advantage of such simplifications. It should be noted that algorithms for orthotropic materials are not developed here. Algorithms for this degree symmetry can be developed by following the same reasoning as is done for transverse isotropy, once the relationships between the independent components are established.

3.3.1 Isotropy or cubic symmetry

As was shown at Sect. 2.3.1, for isotropy or cubic symmetry, a tensor can be expressed as a function of 2 or 3 parameters: $\{\alpha, \beta, \gamma\}$ and the only restriction is that these constants must be positive. They are not related to each other and can therefore be treated independently. Let $\tilde{g}(t)$ be any of these components. Using $\hat{g}(t)$ defined by Eq. (28) leads to the following optimization problem:

$$\inf_{g_n} \sum_{s=1}^{S} \left[\tilde{g}^*(p_s) - \hat{g}(p_s)\right]^2 \quad \text{with } g_n \geq 0$$
$$\text{and} \quad \sum_{n=1}^{N} g_n = \lim_{p\to\infty} \tilde{g}^*(p) \tag{40}$$

This constraint optimization problem can be simplified by defining:

$$\hat{g}(t) = \sum_{n=1}^{N} g_n^2 \exp\left[-t\tau_n\right] \tag{41}$$

and becomes:

$$\inf_{g_n} \sum_{s=1}^{S} \left[\tilde{g}^*(p_s) - \hat{g}^*(p_s)\right]^2 \quad \text{with} \quad \sum_{n=1}^{N} g_n^2 = \lim_{p\to\infty} \tilde{g}^*(p) \tag{42}$$

This problem can be solved with classical optimization tools and the constraint can be imposed with Lagrange Multipliers or with a penalty function.

3.3.2 Transverse isotropy

As shown in Sect. 2.3.2 a transversely isotropic material can be defined by 5 independent constants: $\alpha, \beta, \gamma, \delta$ and δ'. δ and δ' are not related to any other constant and they only need to be positive. These components can therefore be treated in the same way as for the isotropic constants. On the other hand, there is a relationship between α, β and γ and these components must be treated simultaneously.

We define:

$$\hat{\lambda}(t) = \sum_{n=1}^{N} \lambda_n \exp[-t\tau_n] \tag{43}$$

for the approximate functions and:

$$R_\lambda^2 = 1 - \frac{S-1}{S-N-1} \frac{\sum_{s=1}^{S} \left[\tilde{\lambda}^*(p_s^\lambda) - \hat{\lambda}^*(p_s^\lambda)\right]^2}{\sum_{s=1}^{S} \left[\tilde{\lambda}^*(p_s^\lambda) - \left\langle\tilde{\lambda}^*\right\rangle\right]^2} \tag{44}$$

where λ is any of $\{\alpha, \beta, \gamma\}$, the p_s^λ represent the p_s points associated with a λ component and $\langle\lambda\rangle$ represents the average of $\lambda(p_s)$. It can be observed that the approximate functions share the same τ_n. R^2 is the classical coefficient of determination and it is a normalized measure of the discrete differences between the approximate function and the function to be inverted.

The first step here is the determination of the τ_n. We used:

$$\tau_{\min} = \min\{p_1^\alpha, p_1^\beta, p_1^\gamma\} \quad \text{and} \quad \tau_{\max} = \max\{p_s^\alpha, p_s^\beta, p_s^\gamma\} \tag{45}$$

and the τ_n were calculated according to Eq. (37).

The optimization problem that identifies the $\{\alpha_n, \beta_n, \gamma_n\}$ is:

$$\sup_{\{\alpha_n,\beta_n,\gamma_n\}} R_\alpha^2 + R_\beta^2 + R_\gamma^2 \quad \text{with } \alpha_n \geq 0;\ \beta_n \geq 0;\ \gamma_n^2 \leq \alpha_n\beta_n$$
$$\text{and} \quad \sum_{n=1}^{n} \lambda_n = \lim_{p\to\infty} \tilde{\lambda}^*(p) \quad \text{for } \lambda = \{\alpha_n, \beta_n, \gamma_n\} \tag{46}$$

This constraint optimization problem can be simplified with the following change of variables:

$$\alpha_n = x_n^2\ ;\ \beta_n = y_n^2 \ \text{ and } \ \gamma_n = \frac{2}{\pi}\sqrt{x_n^2 y_n^2} \arctan v_n \tag{47}$$

where the variables $\{x_n, y_n, v_n\}$ are those being optimized. When a penalty function is used for the last constraints of Eq. (46) the optimization problem (46) becomes unconstrained and can be solved with classical optimization algorithms. This also leads to an algorithm where two parameters can be adjusted: N and θ.

3.3.3 General anisotropy

The case of general anisotropy is a complex case since the 21 independent components of $\tilde{\mathbf{G}}$ must be optimized simultaneously. It is possible to define an optimization problem as that of Eq. (46) where the 15 angles and the 6 eigenvalues are optimized. When using $\hat{\mathbf{G}}(t)$ as defined by Eq. (39) with 15 terms, this leads to 315 variables to be optimized. This requires considerable computational effort. We have tested an earlier version of our algorithm [26] (see pages 112 and following) on a very simple case. The results obtained were promising. The emphasis of this paper is on testing the performance of our algorithms for a wide range of situations as possible.

Because of the time required for more complex LCT inversions involving a general anisotropic material where the thermodynamics restrictions are enforced, this paper does not deal with this specific case. Such a situation would more suitably be the focus of a separate publication.

3.4 Algorithms for $\mathbf{A}(t)$ and $\mathbf{B}(t)$

Unlike for the homogenized properties, we could not infer the mathematical shape of $\mathbf{A}(t)$ or $\mathbf{B}(t)$. In addition, no thermodynamics restriction is imposed on these functions and therefore, each independent component of these tensors can be treated independently. Experience has shown that using a series of exponentials to approximate the transient part of these tensors is a good choice. Nonetheless, this transient part has to be computed. We have developed in this paper algorithms for relaxation modulus and creep compliance for which the general shapes are given at Eqs. (1, 2). Here, we make the assumption that $\mathbf{A}(t)$ and $\mathbf{B}(t)$ obey Eq. (2b). Since we do not impose any constraint on the sign of the g_n, either form is acceptable. Form (2b) is more general since it contains a viscous term. The algorithm for the inversion of $\mathbf{A}(t)$ and $\mathbf{B}(t)$ is therefore very similar to the one for the inversion of the homogenized properties when thermodynamics restrictions are not enforced.

4 Validation against selected cases

Validation of our algorithms was carried out in two ways: where possible, the approximate function $\hat{g}(t)$ was compared with the exact solution $\tilde{g}(t)$ for each independent component. This was done only for isotropic materials when the analytical solution was known. When the solution was not known analytically, artificial materials were generated and the algorithm tried to invert the LCT of these materials. This allowed comparison with the time domain function for transverse isotropic materials as well as for general anisotropic materials.

We also investigated the correlation between the coefficient of determination R^2 (see Eq. (44)) and a measure of the error (which we define later) in the time domain between the approximate and exact functions. Recall that all our algorithms have two parameters that can be varied: the number N of terms in the approximate function and θ which controls the range over which the τ_n are distributed. The objective here is to introduce an acceptance test for an approximate function (i.e. R^2 should be greater than a particular value) and a way to improve it if it is not acceptable. Here again, the results are shown as a function of material symmetry.

All the algorithms were implemented in the commercial package Mathematica. The optimization problems were solved with the `NMinimize` or `NMaximize` functions within Mathematica.

4.1 Isotropy

4.1.1 Materials simulated

We have tested our algorithms against two homogenization models for which an analytical solution can be obtained: (a) The Mori-Tanaka scheme and (b) the Self-consistent scheme. We also simulated an artificial material obeying the law described by Eq. (5). For each "material" we performed several inversions in order to check the stability of our algorithm.

For the Mori-Tanaka scheme, we simulated a two-phase material with spherical isotropic reinforcements randomly distributed with a volume fraction of 0.3. The solutions used are listed in Wang and Weng [5]. Both phases were viscoelastic with the hydrostatic and deviatoric parts of the compliance obeying:

$$s(t) = \zeta s_1 + \zeta s_2 t + \zeta s_3 (1 - \exp[-t\omega s_4]) \tag{48}$$

where the s_i were random real numbers between 1.0 and 4.0. The parameters ζ and ω controlled the contrast (in the sense of the mechanical properties) between the constitutive phases. For the matrix phase, $\zeta = \omega = 1$ and for the reinforcing phase $\zeta, \omega = \{10, 100, 1000\}$. This was introduced because it was reported by Masson [27] that the contrast between the phases had an influence on the quality of the inversion when using the collocation method. The deviatoric part of the creep compliance of such material is of the form:

$$\bar{s}(t) = \bar{s}_1 + \bar{s}_2 t + \sum_{i=3}^{7} \bar{s}_i (1 - \exp[-t\bar{s}_{i+5}]) \tag{49}$$

where the $\bar{s}_i$ are positive constants. We recall that our algorithms first evaluate $\bar{s}_1$ and $\bar{s}_2$ with limit value theorems and aim at approximating the transient part (i.e. the sum of exponentials). A similar shape is obtained for the hydrostatic part and the transient part is of the same type for the relaxation modulii. Therefore, only the deviatoric part of the creep compliance was studied.

For the Self-consistent scheme, we simulated a two-phase material where the constitutive phases were incompressible and isotropic. The volume fraction of each phase was 0.5 and the morphology was such that no phase played a special role. Each phase r was Maxwellian and its deviatoric part obeyed:

$$\mathrm{dev}(\boldsymbol{\varepsilon}_r)(t) = \zeta a_r \mathrm{dev}(\boldsymbol{\sigma})(t) + \omega T_r \mathrm{dev}(\dot{\boldsymbol{\sigma}})(t) \tag{50}$$

where dev(.) extracts the deviatoric part of its argument and a_r and T_r are random real numbers between 1.0 and 4.0. We have used $\zeta = \omega = 1$ for phase one and $\zeta, \omega = \{10, 100, 1000\}$ for phase two. Homogenization of such a material leads to the following homogenized shear relaxation modulus (for the transient part):

$$\bar{\mu}(t) = \bar{\mu}_1 \exp\left[-\frac{t}{\omega T_1}\right] + \bar{\mu}_2 \exp\left[-\frac{t}{\omega T_2}\right] + \int_0^\infty \breve{\mu}(\tau) \exp\left[-\frac{t}{\tau}\right] \mathrm{d}\tau \tag{51}$$

where $\breve{\mu}(\tau)\mathrm{d}\tau$ is continuous and non-zero for $\tau \in [\tau_1, \tau_2]$ and null elsewhere. In addition $\breve{\mu}(\tau)\mathrm{d}\tau$ meets the thermodynamics restrictions stated in Sect. 2.1. The whole development leading to this result can be found in Beurthey and Zaoui [8]. It is interesting to note here that the homogenized material has a discrete and a continuous relaxation spectra.

For the artificial material, we used the following constitutive theory:

$$\bar{s}(t) = \frac{at}{1 + \zeta bt} \tag{52}$$

where again a, b are random real numbers between 1.0 and 4.0 and $\zeta = \{10, 100, 1000\}$. This material was chosen since it is described with a continuous compliance sprectra for $\tau \in [0, \infty[$ (see Eq. 5).

4.1.2 Simulations

For each material, we have analysed 9 inversions per configuration. For example, for the Mori-Tanaka material, there were two parameters controlling the contrast and each parameter could take three values. This led to 9 configurations. The θ parameter could take 5 values and N could take 4 values. The values used for θ can be found in Table 2 and those for N in Table 3. So, for the Mori-Tanaka scheme we performed $9 \times 3 \times 3 \times 5 \times 4 = 1{,}620$ inversions. This number was the same for the Self-Consistent scheme and for the artificial material we performed 540 inversions (there is only one parameter controlling the contrast). In total, we performed 3,780 inversions.

4.1.3 Evaluation of performance

In order to evaluate the performance of our algorithms and to derive acceptance criteria, we define the following quantity:

$$\tilde{E}^2 = \frac{\int_0^\infty \left[\tilde{g}(t) - \hat{g}(t)\right]^2 \mathrm{d}t}{\int_0^\infty \tilde{g}(t)^2 \mathrm{d}t} \tag{53}$$

which can be interpreted as a normalized measure of the distance between the approximate and exact solution. This is a global indicator of the quality of the inversion. An alternative would have been to use the relative error between $\tilde{g}(t)$ and $\hat{g}(t)$. However, since $\lim_{t\to\infty} \tilde{g}(t) = 0$, this could lead to large relative error even if the absolute difference between the two functions is small. We are interested in the relationship between this measure (which is available only when the exact solution is known) in the coefficient of determination R^2 as calculated from Eq. (44). R^2 is calculated at the end of the inversion and it would be interesting to determine a minimum value for R^2 which would lead to an acceptance/refusal of the inversion thus obtained.

For both versions of the algorithm, a very strong relationship has been observed between R^2 and $\tilde{E}^2$. Figure 3 shows, as an example, the correlation between R^2 and $\tilde{E}^2$ for the Self-Consistent scheme for the algorithm where the thermodynamics restrictions are enforced. The results for the other cases are not reported here since they were similar and led to the same conclusions. From this figure, it seems appropriate to use R^2 to accept or reject an inversion. From these observations, we have set an acceptance criterion to $R^2 = 0.9999$. Table 1 lists the maximum and minimum values of $\tilde{E}^2$ as well as its mean value and a 95% confidence interval.

The worst value of $\tilde{E}^2$ is 3.8×10^{-2}, obtained for the Self-consistent scheme when the thermodynamics restrictions are enforced. For this specific case, the approximate and exact functions are plotted in Fig. 4. The results are remarkably good. It can generally be observed that better results occur when thermodynamics restrictions are not enforced. However, the difference is not very significant. It can also be observed from Fig. 3 and from the width of the confidence intervals on the mean value of $\tilde{E}^2$ in Table 1 that the scatter in the quality of the inversion is considerable.

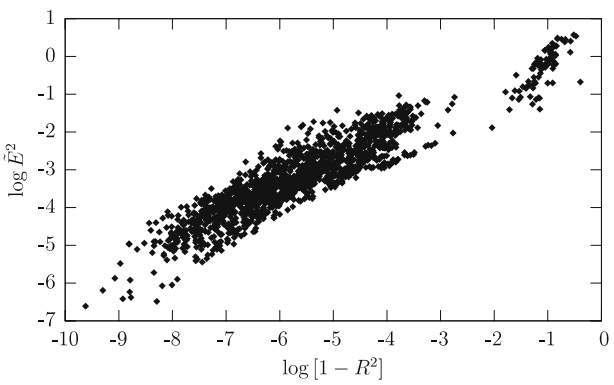

Fig. 3 Correlation between R^2 and $\tilde{E}^2$ for the Self-Consistent scheme for the algorithm where the thermodynamics restrictions are enforced

Table 1 Average and extreme values of $\tilde{E}^2$ obtained for the isotropic materials

	Thermo. restrictions not enforced			Thermo. restrictions enforced		
	MT	SC	Art.	MT	SC	Art.
Max. value	2.9×10^{-2}	2.4×10^{-2}	2.5×10^{-3}	1.91×10^{-2}	3.8×10^{-2}	1.3×10^{-2}
Min. value	3.1×10^{-15}	3.0×10^{-15}	2.3×10^{-4}	3.8×10^{-7}	2.5×10^{-7}	5.3×10^{-4}
Sup. bound	2.6×10^{-4}	4.2×10^{-4}	1.1×10^{-3}	6.3×10^{-4}	2.3×10^{-3}	2.0×10^{-3}
Mean value	2.0×10^{-4}	3.4×10^{-4}	1.0×10^{-3}	5.8×10^{-4}	2.0×10^{-3}	1.8×10^{-3}
Inf. bound	1.4×10^{-4}	2.6×10^{-4}	1.0×10^{-3}	5.2×10^{-4}	1.8×10^{-3}	1.7×10^{-3}

Sup. and Inf. bounds refer to the upper and lower 95% confidence intervals on the mean value. MT refers to the Mori-Tanaka material, SC to the Self-Consistent and Art. to the artificial material. The confidence intervals for MT and SC are based on 1620 observations and on 540 for Art

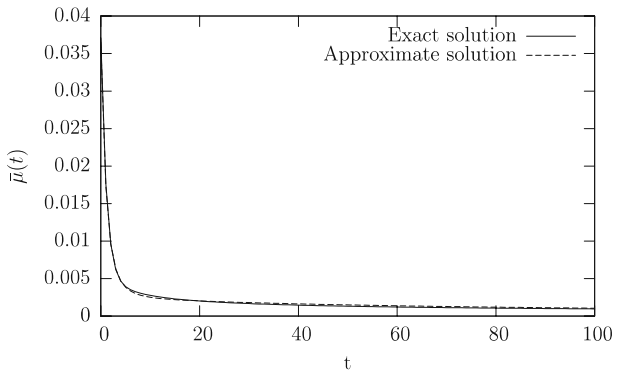

Fig. 4 Comparison between the exact solution and the approximate solution for the largest value of $\tilde{E}^2$ obtained for the isotropic cases simulated. This *curve* was obtained for a value of $\tilde{E}^2 = 3.76 \times 10^{-2}$ for the Self-consistent scheme when the thermodynamics restrictions are enforced

It is also of interest to study the influence of the parameter θ and N on the quality of the inversion. Tables 2 and 3 list the mean value of the inversions for different values of θ and N. It should be noted here that all the inversions were used to generate these estimates (i.e., even those where $R^2 < 0.9999$). This was done in order to identify the parameters which are more likely to lead to an acceptable inversion.

It is difficult to draw conclusions on the value of θ. From one model to the next, any trends that are apparent can be contradictory. For N, on the other hand, the trends are more clear. It seems that the worse results are obtained for 10 or 25 terms in the approximate function. It would seem that 10 terms, on average, are not sufficient to capture the behavior of the whole material with the actual algorithm. On the other hand, the same reasoning cannot be applied to 25 terms since using 15 or 20 terms leads to better results. For the cases where the thermodynamics restrictions are not enforced, we have observed that those cases where 25 terms were used showed oscillations in the time domain. This is due to the fact that the g_n can take either a positive or a negative value. As the number of terms in the approximate function increases, the possibility of obtaining oscillations increases. For algorithms where the thermodynamics restrictions are enforced, such reasoning does not apply and the reasons for this phenomenon are not clear. One possible explanation is that the optimization algorithm finds a local optimum rather than an absolute optimum. As the number of terms increases,

Table 2 Influence of the parameter θ on the quality of the inversion for the isotropic materials

	Value of the parameter θ				
	$\frac{1}{100}$	$\frac{5}{100}$	$\frac{9}{100}$	$\frac{13}{100}$	$\frac{17}{100}$
N. enf.					
MT ($\times 10^{-4}$)	1.1 ± 0.5	0.8 ± 0.3	0.7 ± 0.3	1.5 ± 0.6	5.9 ± 2.7
SC ($\times 10^{-4}$)	1.4 ± 0.7	1.8 ± 0.9	2.7 ± 1.2	4.2 ± 1.9	6.9 ± 2.9
Art. ($\times 10^{-3}$)	0.68 ± 0.07	0.80 ± 0.08	0.96 ± 0.09	1.2 ± 0.1	1.6 ± 0.1
Enf.					
MT ($\times 10^{-2}$)	6.6 ± 4.6	3.9 ± 3.0	4.8 ± 4.0	3.9 ± 3.2	3.2 ± 2.2
SC ($\times 10^{-2}$)	7.3 ± 4.2	6.7 ± 3.4	3.5 ± 1.8	3.5 ± 2.7	2.0 ± 1.2
Art. ($\times 10^{-3}$)	1.4 ± 0.2	8.2 ± 13.1	2.1 ± 0.4	1.9 ± 0.2	2.3 ± 0.2

"N. enf" and "Enf." refer to algorithms where the thermodynamics restrictions are not and are enforced, respectively. *MT* refers to the Mori-Tanaka scheme, "SC" to the Self-Consistent scheme and "Art." to the artificial material. The results are the mean value of $\tilde{E}^2$ and its 95% confidence interval. The confidence intervals for MT and SC are based on 324 observations and on 108 for Art

Table 3 Influence of the parameter N on the quality of the inversion for the isotropic materials

	Number of terms in the approximate function			
	10	15	20	25
N. enf.				
MT ($\times 10^{-4}$)	2.1 ± 0.5	0.27 ± 0.08	0.9 ± 0.4	4.7 ± 2.8
SC ($\times 10^{-3}$)	1.0 ± 0.3	0.3 ± 0.1	0.04 ± 0.02	0.005 ± 0.004
Art. ($\times 10^{-3}$)	1.76 ± 0.07	1.18 ± 0.06	0.73 ± 0.04	0.46 ± 0.02
Enf.				
MT ($\times 10^{-2}$)	1.8 ± 0.7	0.04 ± 0.006	1.0 ± 1.7	15.0 ± 5.8
SC ($\times 10^{-2}$)	16.6 ± 4.6	0.4 ± 0.2	0.22 ± 0.05	1.1 ± 1.8
Art. ($\times 10^{-3}$)	7.5 ± 10.4	2.1 ± 0.1	1.9 ± 0.3	1.3 ± 0.2

"N. enf" and "Enf." refer to algorithms where the thermodynamics restrictions are not and are enforced, respectively. *MT* refers to the Mori-Tanaka scheme, "SC" to the Self-consistent scheme and "Art." to the artificial material. The results are the mean value of $\tilde{E}^2$ and its 95% confidence interval. The confidence intervals for MT and SC are based on 405 observations and on 135 for Art

the possibility of finding a local optimum also increases. This problem is not present with the algorithm where the thermodynamics restrictions are not enforced since the optimization problem is linear (i.e. the optimum is unique). From these observations, it would seem that using 15 or 20 terms for the approximate function is a good choice.

We have performed a similar analysis to study the effect of the contrast (parameters ζ and ω). As for the parameter θ, it was not possible to draw clear conclusions regarding the influence of these parameters on the quality of the inversion.

In conclusion, for the isotropic materials studied here, it would seem appropriate to use $R^2 \geq 0.9999$ as an acceptance criteria for the inversion. Algorithm 2 summarizes the required steps.

Algorithm 2 Inversion for isotropy or cubic symmetry when thermodynamics restrictions are enforced

```
Obtain the permanent and transient parts according to Eqs. (31).
for α, β, γ do
  repeat
    for all the Nτ different values of N do
      Compute the p_s according to Algorithm 1 (if required).
      for all the Nθ different values of θ do
        Compute the τ_n according to Equation (37).
        Solve Equation (40).
        Compute R^2.
      end for
    end for
  until R^2 ≥ 0.9999
end for
```

4.2 Inversions for **A** and **B**

4.2.1 Simulations

We have applied our algorithms to the deviatoric part of the strain localization tensor **A** and stress concentration tensor **B** for the matrix phase for the Mori-Tanaka Scheme (these tensors are isotropic). The materials used were the same as described in Sect. 4.1.1 and the simulations were similar to those described in Sect. 4.1.2: we performed 8 repetitions per simulation instead of 9. This led to 1,440 inversions for each **A** and **B**.

The deviatoric part of $\mathbf{A}_0$ is of the type:

$$A_0^d(t) = s_1 + \sum_{i=2}^{7} s_i \exp\left[-tz_i\right] \tag{54}$$

and the deviatoric part of $\mathbf{B}_0$ is of the type:

$$B_0^d(t) = s_1 + \sum_{i=2}^{4} s_i \exp\left[-tz_i\right] \tag{55}$$

where the s_i are real constants that can take either negative or positive values and the z_i are positive constants.

4.2.2 Evaluation of performance

We recall that there is no thermodynamics restriction for these tensors. Therefore, the function can take positive as well as negative values and exhibit some oscillations. It was found that $R^2 \geq 0.9999$ was not a good acceptance criterion since when it was applied, solutions where $\tilde{E}^2$ was unacceptable were kept. On the other hand, it was found that it was a good criterion to reject solutions: in other words, inversions where $R^2 < 0.9999$ led to unacceptable values of $\tilde{E}^2$.

When observing the cases where a solution with an unacceptable value of $\tilde{E}^2$ were accepted, it was found that the approximate and exact functions in the Laplace–Carson space were almost identical. On the other hand, in the time domain, the approximate function showed more oscillations than the exact solution. For illustration

purposes, consider the simple function:

$$f(t) = -a\exp[-bt] + c\exp[-\mathrm{d}t] \tag{56}$$

where all the constants are positive. The point t_o where this function will show oscillation is the point where its slope is zero (besides at infinity). For this simple case, this point is:

$$t_o = \frac{\ln[ba] - \ln[dc]}{b - d} \tag{57}$$

and depending on the value of the parameters, t_o can either be positive or negative. With the same function, the points p_o where the slope of its LCT is zero are the roots of the following equation (this can be obtained by very simple algebraic manipulations):

$$cdb^2 - abd^2 + 2\,(bcd - abd)\,p_o + (cd - ab)\,p_o^2 = 0 \tag{58}$$

again, depending on the values of the constants, p_o can be positive, negative or complex. There is no direct relationship between t_o and p_o and therefore it is possible to have a $t_o > 0$ and $p_o < 0$. This can explain why an acceptable value of R^2 could lead to an unacceptable value of $\tilde{E}^2$.

For each exact function for which the approximate function was sought, 20 inversions were performed (combinations of 5 values of θ and 4 values of N). It was observed for each exact function being inverted that a large number of these 20 inversions led to very similar values of $\tilde{E}^2$ and these values were very good values. In other words, our algorithm, almost, leads to an acceptable solution. The key issue is now how to eliminate the unacceptable solutions from the acceptable solutions.

Since the acceptable solutions are similar, one possible way to distinguish them is to compare the following quantity:

$$E^{\infty} = \int_0^{\infty} \left(\hat{g}(t)\right)^2 \mathrm{d}t = \sum_{i=1}^{N}\sum_{j=1}^{N} \frac{g_i g_j}{\tau_i + \tau_j} \tag{59}$$

E^{∞} can be obtained with very simple operations. If one approximate solution presents some important oscillations, its value of E^{∞} will be different from the others. So, the algorithm here would be to generate a number R of inversions and compare them to each other and keep the solutions which are close to each other. To accomplish this we defined the following comparison criterion:

$$\Phi_{ij} = \left| \frac{E_i^{\infty} - E_j^{\infty}}{\min\left\{E_i^{\infty}, E_j^{\infty}\right\}} \right| \tag{60}$$

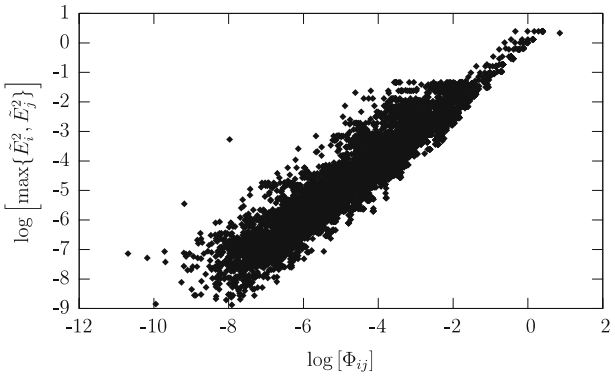

Fig. 5 $\log\left[\max\left\{\tilde{E}_i^2, \tilde{E}_j^2\right\}\right]$ as a function of $\log \Phi_{ij}$ obtained for $\mathbf{A}_0$

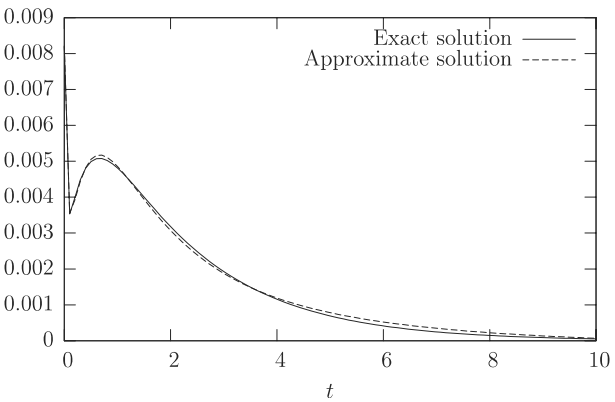

Fig. 6 Comparison between the approximate and exact solution for the transient deviatoric part of $\mathbf{B}_0$ for $E^2 = 4.9 \times 10^{-3}$

This leads to $R(R-1) - \sum_{i=1}^{R-1} i$ comparisons. Figure 5 shows $\log\left[\max\left\{\tilde{E}_i^2, \tilde{E}_j^2\right\}\right]$ as a function of $\log \Phi_{ij}$ for the results obtained for $\mathbf{A}_0$. As can be seen, there is a strong correlation between these two quantities and this shows that Φ_{ij} can be used as an acceptance criterion. We accepted a solution when $\Phi_{ij} \leq 10^{-5}$. A similar plot has been obtained for $\mathbf{B}_0$ and is not reported here.

When this acceptance criterion is applied (in addition to the first screening with R^2), the maximum value of $\tilde{E}^2$ we obtained for $\mathbf{A}_0$ was 7.0×10^{-4} and for $\mathbf{B}_0$ was 4.9×10^{-3}. Figure 6 illustrates this last result. It should be noted that for one case, it was not possible to find an acceptable solution with this acceptance criterion (after 20 inversions). In that case, using the lowest value of Φ_{ij} led to an acceptable result ($\tilde{E}^2 = 4.1 \times 10^{-5}$). The algorithm for these tensors is summarized as Algorithm 3.

As for the homogenized properties, we have conducted an analysis of the influence of the parameters N and θ as well as the contrast between the phases on the mean value of $\tilde{E}^2$ for all the inversions. For both tensors $\mathbf{A}_0$ and $\mathbf{B}_0$ only the parameter N had a statistically significant influence on $\tilde{E}^2$. Table 4 lists these results. All the simulations were used to compute the mean values.

Table 4 Effect of the number of terms in the approximate function on the mean value of $\tilde{E}^2$

	Number of terms in the approximate function			
Tensor	10	15	20	25
$\mathbf{A}_0$	$2.5 \pm 1.7 \times 10^{-2}$	$4.7 \pm 2.6 \times 10^{-4}$	$2.3 \pm 1.1 \times 10^{-5}$	$9.9 \pm 3.6 \times 10^{-7}$
$\mathbf{B}_0$	$4.5 \pm 2.1 \times 10^{-2}$	$1.9 \pm 1.0 \times 10^{-3}$	$1.2 \pm 0.9 \times 10^{-4}$	$5.0 \pm 3.1 \times 10^{-6}$

The tolerance represents a 95% confidence interval. The confidence intervals are based on 360 observations

Algorithm 3 Inversion when thermodynamics restrictions are not enforced

```
Obtain the permanent and transient parts according to Eqs. (31).
for all the independent components do
  repeat
    for all the Nτ different values of N do
      Compute the p_s according to Algorithm 1 (if required).
      for all the Nθ different values of θ do
        Compute the τ_n according to Eq. (37).
        Solve Equation (38).
        Compute R^2 and E^∞.
        if R^2 ≥ 0.9999 then
          Store E^∞ for this inversion.
          Compute Φ_ij for this new inversion with all the other inversions stored at the preceeding steps.
        end if
      end for
    end for
  until Φ_ij ≤ 10^-5
end for
```

Again, it can be observed from Table 4 that the scatter in the results is considerable since it leads to large confidence intervals with respect to the mean value. It should be noted that such an algorithm could be applied to the homogenized properties of isotropic materials when the thermodynamics restrictions are not enforced. Even though it was observed for the cases simulated that $R^2 \geq 0.9999$ is a relevant acceptance criterion, using Algorithm 3 would diminish the possibility of accepting an over-oscillating solution.

It should also be noted that this algorithm requires many operations. The most computationally demanding is the determination of the p_s since it is a nonlinear process. Computing the g_n is equivalent to solving an $N \times N$ linear system of equations which can be solved very efficiently. So, once the p_s are obtained, generating many inversions by varying θ can be done in a very short execution time.

4.3 Inversions for transverse isotropic tensors

4.3.1 Simulations

As stated in Sect. 2.3.2, the parameters δ and δ' have the same restrictions as the scalars used in the short hand notation for isotropic tensors. Since we already developed and tested algorithms for similar components, δ and δ' were not tested here. The algorithms are then tested only on the parameters α, β and γ since they are related to each other.

We have simulated artificial homogenized materials in order to test our algorithms. We have used materials where the transient part was described with five transversly isotropic tensors multiplying a decaying exponential, as in Eq. (39). We have generated the following functions:

$$\begin{aligned}
\alpha(t) &= \sum_{i=1}^{5} s_i \exp[-\tau_i t] \\
\beta(t) &= \sum_{i=1}^{5} z_i \exp[-\tau_i t] \\
\gamma(t) &= \sum_{i=1}^{3} w_i \exp[-\tau_i t] + \sum_{i=4}^{5} v_i \exp[-\tau_i t]
\end{aligned} \tag{61}$$

where s_i and z_i are random numbers between 0 and 50.0, w_i are random numbers between 0 and $\sqrt{s_i z_i}$, v_i are random numbers between $-\sqrt{s_i z_i}$ and $\sqrt{s_i z_i}$ and τ_i are randomly distributed, on a log scale, between 0.01 and 100.0.

We have tested 40 different materials and used the same θ and N parameters as in the case of isotropy.

4.3.2 Performance when the thermodynamics restrictions are not enforced

We have applied the same acceptance criteria as developed for the tensors $\mathbf{A}(t)$ and $\mathbf{B}(t)$ for each of $\hat{\alpha}$, $\hat{\beta}$ and $\hat{\gamma}$. In total, $3 \times 40 \times 4 \times 5 = 2,400$ separate inversions were performed. The worst value of $\tilde{E}^2$ accepted (after the acceptance criterion as described at Algorithm 3) was 4.56×10^{-3} (obtained for $\alpha(t)$). A plot of this latter inversion leads to a graph of comparable accuracy as that of Fig. 6 and is not reported here.

As for the tensors $\mathbf{A}(t)$ and $\mathbf{B}(t)$, the number of terms in the approximate function has a significant influence on the quality of the inversion. This result could be expected since the shape of the exact function in both cases

Table 5 Effect of the number of terms in the approximate function on the mean value of $\tilde{E}^2$ for the a transversely isotropic material where the thermodynamics restrictions are not enforced. The tolerance represents a 95% confidence interval. The confidence intervals are based on 200 observations

	Number of terms in the approximate function			
Component	10	15	20	25
α	$4.9 \pm 1.1 \times 10^{-4}$	$8.8 \pm 3.1 \times 10^{-6}$	$1.7 \pm 0.9 \times 10^{-7}$	$6.6 \pm 1.5 \times 10^{-8}$
β	$5.4 \pm 1.8 \times 10^{-4}$	$7.0 \pm 2.7 \times 10^{-6}$	$1.3 \pm 0.4 \times 10^{-8}$	$7.0 \pm 1.4 \times 10^{-8}$
γ	$3.6 \pm 1.2 \times 10^{-3}$	$1.2 \pm 0.6 \times 10^{-4}$	$8.3 \pm 7.4 \times 10^{-6}$	$3.6 \pm 2.9 \times 10^{-7}$

Table 6 Effect of the parameter θ on the mean value of $\tilde{E}^2$ for a transversely isotropic material where the thermodynamics restrictions are not enforced

	Value of the parameter θ				
Component	1/100	5/100	9/100	13/100	17/100
$\alpha(\times 10^{-4})$	2.2 ± 1.0	1.5 ± 0.8	1.1 ± 0.7	0.8 ± 0.5	0.6 ± 0.3
$\beta(\times 10^{-4})$	3.1 ± 1.9	1.8 ± 1.2	1.0 ± 0.6	0.6 ± 0.3	0.4 ± 0.2
$\gamma(\times 10^{-3})$	1.6 ± 0.9	1.0 ± 0.8	0.8 ± 0.7	0.7 ± 0.6	0.6 ± 0.5

The tolerance represents a 95% confidence interval. The confidence intervals are based on 160 observations

is very similar. Table 5 lists the results. Again, the scatter in the results is considerable.

We have also observed that the parameter θ, in these cases, had a statistically significant influence on the quality of the inversion for the parameters α and β but not for γ. Table 6 lists these results. All the simulations were used to compute the mean values.

4.3.3 Performance when the thermodynamics restrictions are enforced

For this algorithm, it was not possible to obtain inversions where R^2 was superior to 0.9999 simultaneously for all of α, β and γ, for all the 40 materials we have tested. This suggests that the quality of the inversion for this algorithm should be less than for the algorithm where the thermodynamics restrictions were not enforced.

In order to accept a solution, we relaxed our tolerance on the value of R^2 by rejecting inversions where R^2 was not superior to 0.999 simultaneously for all α, β and γ. Then, as we have done for tensors **A** and **B**, we only kept those solutions where $\Phi_{ij} \leq 10^{-2}$ for the parameter γ. Then, from the remaining solutions, the solution where the minimum value of R^2 for α, β and γ was the largest (for a given material) was chosen as the final solution. Algorithm 4 lists the steps we have followed.

When this process was applied, it was not possible to obtain a solution for 3 of the 40 materials. It is possible that performing more inversions for the same material (using more values for θ or N) could have improved the results. The largest value of $\tilde{E}^2$ accepted with this process was 0.13 (obtained for α), which is quite large in comparison to the values obtained before. Figure 7 shows an example of the difference between the exact and approximate function that can be obtained.

It was found that the parameter θ did not have a statistically significant influence on the quality of the inversion. On the other hand, the number of terms in the

Algorithm 4 Inversion for transverse isotropy when the thermodynamics restrictions are enforced

1: Obtain the permanent and transient parts according to Eqs. (31).
2: **for** δ, δ' **do**
3: Perform the inversion as per Algorithm 2.
4: **end for**
5: **for** all the $N\tau$ different values of N **do**
6: Compute the p_s according to Algorithm 1 (if required) for α, β and γ.
7: **for** all the $N\theta$ different values of θ **do**
8: Compute τ_{min} and τ_{max} according to Eq. (45).
9: Compute the τ_n according to Equation (37).
10: Solve Equation (46).
11: Compute R^2 and E^{∞}.
12: **end for**
13: **end for**
14: **for** all the $N\tau \times N\theta$ inversions **do**
15: Keep the inversions for which $R^2 \geq 0.999$ simultaneously for α, β and γ.
16: **end for**
17: **for** the γ component of all the remaining inversions **do**
18: Keep the inversions for which $\Phi_{ij} \leq 10^{-2}$.
19: **end for**
20: Select as a solution the inversion for which the lowest value of R^2 associated with α, β and γ is the largest.

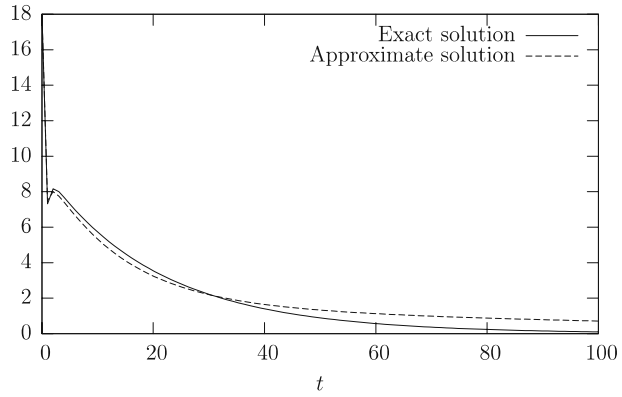

Fig. 7 Comparison between the approximate and exact functions for γ for $\tilde{E}^2 = 5.4 \times 10^{-2}$ for a transversly isotropic material when the thermodynamics restrictions are enforced

approximate function had a statistically significant influence. This influence is, however, less important than the one observed for the other cases studied so far. Table 7 lists these results. All the simulations were used to compute the mean values.

4.4 Inversions for anisotropic tensors

4.4.1 Simulations

We have generated artificial anisotropic materials from Eqs. (14–16). We have simulated materials obeying the general form of Eq. (39) with 5 terms. The τ_n of Eq. (39) were randomly distributed, on a log scale, between 0.01 and 100.0. The θ_i of Eq. (15) were randomly generated between 0 and 2π. The diagonal components of the matrix $\mathbf{D}$ of Eq. (14) were random numbers between 0 and 100.

We have generated 20 different anisotropic materials. Since each of the 21 components is treated independently, we have in fact applied the algorithm to 420 1D materials.

4.4.2 Evaluation of performance

We have applied Alogorithm 3 to all the 420 1D materials. In total, it was not possible to obtain a solution for 4 materials out of the 420 with the selection criteria of Algorithm 3. However, for these four cases, selecting the lowest value of Φ_{ij} led to acceptable results. The maximum value of $\tilde{E}^2$ accepted was $\tilde{E}^2 = 1.2 \times 10^{-2}$, which is acceptable (we have already shown plots for similar values of $\tilde{E}^2$).

As for the other algorithms, it was found that the number of terms in the approximate function had a statistically significant influence on the value of $\tilde{E}^2$. Table 8 lists the results. It was also found that the parameter θ had a statistically significant influence on the value of $\tilde{E}^2$. However, this influence is not very strong. Table 9 lists the results. All the simulations were used to compute the mean values.

5 Discussion and conclusion

We have developed algorithms inverting the Laplace–Carson transforms involved in the homogenization of viscoelastic materials. The algorithms introduce acceptance criteria for the inversions and thus lead to solutions of very good quality. This is a major improvement on previously existing algorithms. We have also introduced algorithms which allow homogenized properties to be obtained whilst meeting the thermodynamics require-

Table 7 Effect of the number of terms in the approximate function on the mean value of the sum of $\tilde{E}^2$ associated with α, β and γ for the a transversely isotropic material where the thermodynamics restrictions are enforced

	Number of terms in the approximate function			
Component	10	15	20	25
$\alpha + \beta + \gamma (\times 10^{-2})$	3.9 ± 1.3	2.1 ± 0.7	2.0 ± 0.4	2.1 ± 0.5

The tolerance represents a 95% confidence interval. The confidence intervals are based on 200 observations

Table 8 Effect of the number of terms in the approximate function on the mean value of $\tilde{E}^2$ for the anisotropic materials where the thermodynamics restrictions are not enforced

Number of terms in the approximate function			
10	15	20	25
$1.6 \pm 0.5 \times 10^{-2}$	$5.5 \pm 1.8 \times 10^{-4}$	$5.6 \pm 2.5 \times 10^{-5}$	$3.6 \pm 3.0 \times 10^{-5}$

The tolerance represents a 95% confidence interval. The confidence intervals are based on 2,100 observations

Table 9 Effect of the parameter θ on the mean value of $\tilde{E}^2$ for the anisotropic materials where the thermodynamics restrictions are not enforced

Value of the parameter θ				
$\frac{1}{100}$ ($\times 10^{-3}$)	$\frac{5}{100}$ ($\times 10^{-3}$)	$\frac{9}{100}$ ($\times 10^{-3}$)	$\frac{13}{100}$ ($\times 10^{-3}$)	$\frac{17}{100}$ ($\times 10^{-3}$)
9.2 ± 5.3	5.4 ± 3.1	3.3 ± 1.9	2.0 ± 1.2	1.3 ± 0.7

The tolerance represents a 95% confidence interval. The confidence intervals are based on 1,680 observations

ments. This is another improvement on previous algorithms.

We have tested our algorithms on different homogenization schemes and on different materials. For all the algorithms where thermodynamics restrictions were not enforced, we obtained very good results. We also obtained very good results for isotropic materials where the thermodynamics restrictions were enforced. However, we obtained results that were only acceptable for the transversely isotropic materials we have tested. This might be due to the fact that the algorithm involves a nonlinear optimization problem where the number of variables is quite important. The quality of the inversion depends on the optimization algorithm used. It can be expected that such problems will be amplified for anisotropic materials where the number of variables to optimize is considerable. The choice of the best optimization algorithm for this class of problems has not been studied in this paper. This matter should be studied if our current algorithms enforcing the thermodynamics restrictions are to be improved.

The algorithms suggested in this paper depend on two parameters: N, the number of terms in the approximate function and θ, which controls the range over which the characteristic times (i.e. the τ_n) are distributed. For all the cases we have studied, it was found that N had a significant influence on the quality of the inversion and usually, a larger N led to better results. It was found, however, in some situations that using 25 terms in the approximate function can lead to a large number of oscillations and therefore to bad results. Based on our observations, it would seem that $N \in [15, 20]$ is a good choice. It was observed for the parameter θ that, in some circumstances, it had an influence on the quality of the inversion and in some other cases it had not. Therefore, based on our observations, it is not possible to draw conclusions regarding the influence of this parameter. The parameter θ can then be interpreted as a statistical variable which allow inversions to be generated (for the same material) from which acceptable solutions are chosen.

It should be recalled that the algorithms developed here are based on the assumption that the transient part of exact function vanished at infinity. If this condition is not met, then our algorithms will fail to find appropriate solutions. In order to treat such cases with our algorithms, it would be necessary to change the form of the approximate function. This could also be done in future work.

Finally, it should be pointed out that the scatter in the quality of the inversion was important for each case tested in this paper. We have obtained good results with the acceptance criteria we have defined. Although it would seem to be rare, considering the amount of testing we have conducted, it could be possible that an unacceptable solution be accepted with our algorithms. This is a limitation of the work presented in this paper.

Acknowledgments The useful discussions with and advice of Pierre Gilormini are greatly acknowledged. Part of this work was funded by the Fonds Québécois de la Recherche sur la Nature et les Technologies and by Enterprise Ireland (Grant PRP00/MI/11).

References

1. Eshelby JD (1957) The determination of the elastic field of an ellipsoidal inclusion and related problems. Proc R Soc Lond Ser A 241:376–396
2. Hershey AV (1954) The elasticity of an isotropic aggregate of anisotropic cubic crystals. J Appl Mech 21:236–240
3. Hashin Z (1966) Viscoelastic fibre reinforced materials. AIAA J 4(8):1411–1417
4. Laws N, McLaughlin R (1978) Self-consistent estimates for the viscoelastic creep compliances of composite materials. Proc R Soc Lond A 359:251–273
5. Wang YM, Weng GJ (1992) The influence of inclusion shape on the overall viscoelastic behavior of composites. J Appl Mech 59:510–518
6. Rougier Y, Stolz C, Zaoui A (1993) Représentation spectrale en viscoélasticité linéaire des matériaux hétérogènes. Comptes Rendus Acad Sci 316(Série II b):1517–1522
7. Brinson LC, Lin WS (1998) Comparison of micromechanics methods for effective properties of multiphase viscoelastic composites. Composites Struct 41:353–367
8. Beurthey S, Zaoui A (2000) Structural morphology and relaxation spectra of viscoelastic heterogeneous materials. Eur J Mech A/Solids 19:1–16
9. Turner PA, Tomé CN (1993) Self-consistent modeling of visco-elastic polycrystals: application to irradiation creep and growth. J Mech Phys Solids 41(7):1191–1211

10. Li J, Weng GJ (1997) A secant-viscosity approach to the time-dependent creep of an elastic-viscoplastic composite. J Mech Phys Solids 45(7):1069–1083
11. Masson R, Zaoui A (1999) Self-consistent estimates for the rate dependent elastoplastic behaviour of polycrystalline materials. J Mech Phys Solids 47:1543–1568
12. Brenner R, Masson R, Castelneau O, Zaoui A (2002) A "quasi-elastic" affine formulation for the homogenised behaviour of nonlinear viscoelastic polycrystals and composites. Eur J Mech A/Solids 21:943–960
13. Lévesque M, Derrien K, Mishnaevsky L, Jr, Baptiste D, Gilchrist MD (2004) A micromechanical model for nonlinear viscoelastic particle reinforced polymeric composite material–undamaged state. Composites Part A Appl Sci Manuf 35(7–8):905–913
14. Biot MA (1954) Theory of stress–strain relations in anisotropic viscoelasticity and relaxation phenomena. J Appl Phys 25(1):1385–1391
15. Bouleau N (1992) Interprétation probabiliste de la viscoélasticité linéaire. Mech Res Commun 19:15–20
16. Bouleau N (1999) Viscoélasticité et processus de lévy. J Potential Anal 11(3):289–302
17. Hill R (1965) Continuum micro-mechanics of elastoplastic polycrystals. J Mech Phys Solids 13:89–101
18. Mori T, Tanaka K (1973) Average stress in matrix and average elastic energy of materials with misfitting inclusions. Acta Metallurgica Materialia 21:597–629
19. Walpole LJ (1981) Elastic behavior of composite materials: theoretical foundations. Adv Appl Mech 21:169–242
20. Bornert M, Bretheau T, Gilormini P (2001) Homogénéisation en mécanique des matériaux 2 – Comportements non linéaires et problèmes ouverts. Hermès Science Publications, Paris
21. Gavazzi AC, Lagoudas DC (1990) On the numerical evaluation of Eshelby's tensor and its application to elastoplastic fibrous composites. Comput Mech 7:13–19
22. Davies B, Martin B (1979) Review – numerical inversion of the Laplace transform: a survey and comparison of methods. J Comput Phys 33:1–32
23. Schapery RA (1962) Approximate methods of transform inversion for viscoelastic stress analysis. In: Proceedings of the 4th US national congress on applied mechanics, vol 2, pp 1075–1085
24. Cost TL, Becker EB (1970) A multidata method of approximate Laplace transform inversion. Int J Numer Methods Eng 2:207–219
25. Press WH, Teukolsky SA, Vetterling, WT, Flannery BP (2001) Numerical Recipes in Fortran 77 : the art of scientific Computing. Cambridge University Press, Cambridge
26. Lévesque M (2004) Modélisation du comportement mécanique de matériaux composites viscoélastiques non linéaires par une approche d'homogénéisation. PhD thesis, École Nationale Supérieure d'Arts et Métiers, Paris In English, download at `pastel.paristech.org/archive/00001237/`
27. Masson R (1998) Estimations non linéaires du comportement global de matériaux hétérogènes en formulation affine: application aux alliages de zirconium. PhD Thesis, Ecole Polytechnique, Paris